Mechanics Research Communications 103 (2020) 103463

Contents lists available at ScienceDirect

Mechanics Research Communications

journal homepage: www.elsevier.com/locate/mechrescom

Shape memory response and hierarchical motion capabilities of 4D printed auxetic structures

Stefano Pandini[a], Nicoletta Inverardi[a], Giulia Scalet[b,*], Davide Battini[a], Fabio Bignotti[a], Stefania Marconi[b], Ferdinando Auricchio[b]

[a] Department of Mechanical and Industrial Engineering, University of Brescia, via Branze 38, Brescia, 25133, Italy
[b] Department of Civil Engineering and Architecture, University of Pavia, via Ferrata 3, Pavia, 27100, Italy

ARTICLE INFO

Article history:
Received 28 June 2019
Revised 22 October 2019
Accepted 3 December 2019
Available online 5 December 2019

Keywords:
4D printing
Auxetics
Metamaterials
Shape memory polymers
Temperature memory effect

ABSTRACT

4D printing refers to a novel trend in the field of active materials, regarding the employment of additive manufacturing to obtain structures presenting inherent complex shapes and shape evolutions under the application of proper stimuli. Such a technique is a powerful tool to realize auxetic structures with customized architectures and programmable/controllable shape change. The present paper proposes 4D printed shape memory polymer-based systems with auxetic structure, capable of hierarchical motion. The systems were prepared starting from a commercial photopolymer by means of stereolithography. The mechanical behavior of the systems was characterized in uniaxial tensile tests, measuring the strains parallel/perpendicular to the load direction. Thanks to a broad glass transition region, the photopolymer displays the so-called "Temperature-Memory Effect" (TME), i.e. the possibility to tailor the thermal trigger of the Shape-Memory Effect (SME) through the deformation temperature. Thermo-mechanical histories were applied to a single unit cell to investigate both the overall shape memory response and the possibility to undergo multiple combined out-of-plane and in-plane motions on the basis of the TME. Obtained results allow discussing the effect of deformation temperatures on the thermal region triggering the SME and show the possibility to exploit the TME to achieve sequential self-deployment of auxetic structures.

1. Introduction

Mechanical metamaterials are artificial structures exhibiting unusual macroscopic properties due to their rationally-designed architecture. Thanks to their peculiar properties, metamaterials are promising candidates for several applicative fields, e.g. soft robotics/electronics, medicine, and acoustic cloaking.

In particular, negative Poisson's ratio materials, also known as auxetics, represent one of the most studied type of mechanical metamaterials. Thanks to the negative Poisson's ratio effect, auxetics possess, in fact, advanced functionalities such as high penetration resistance, enhanced fracture toughness, tunable energy absorption, and synclastic curvature upon flexure [1].

Once manufactured, these auxetic structures do not generally change their configuration in response to application needs, and, reasonably, the same holds for their functionalities. On the contrary, greater flexibility and adaptability may be achieved in auxetics having a reversibly tunable, programmable, and controllable structure, in addition to the functionalities listed above. Such a behavior may be beneficial for various applications, for example, for the realization of shape-matching materials to be used in soft robotics and wearable medical devices [2] or for aerospace deployable antennas [3].

A common approach to realize tunable and programmable auxetics is to promote important structural changes by exploiting mechanisms such as multi-stability and buckling (see, e.g. [4]). However, such an approach usually requires the intervention of external mechanical loads, actuators, and/or viscoelastic effects to activate the different designed configurations.

To overcome such a limit, a possible solution is to use active materials, able to respond to an external stimulus (temperature, magnetic fields, humidity, etc.) by significant shape variations. These changes may involve also articulated types of shape variations, e.g. sequential motion, that is at the basis of the development of smart self-folding and self-deploying structures [3,5].

In the last years, the interest towards such an approach has been boosted by the considerable advances in 4D printing tech-

* Corresponding author.
E-mail address: giulia.scalet@unipv.it (G. Scalet).

https://doi.org/10.1016/j.mechrescom.2019.103463
0093-6413/

nology [6], which has been shown to be a powerful tool to realize, through additive manufacturing, auxetic structures with arbitrarily complex or customized architectures (difficult to realize with traditional manufacturing processes) and capable of additional shape transformation along time (denoting the 4th dimension) under the application of proper stimuli. The 4D printed materials used to realize programmable auxetics range from functional polymers [7–12] and magneto-rheological fluid suspensions [13] to shape memory alloys [14]. In particular, Shape-Memory Polymers (SMPs) exhibiting the one-way Shape-Memory effect (SME), that is the ability to return from a deformed temporary shape to the original permanent shape through the application of a thermal stimulus, are the most studied active materials. Various printing techniques were employed: Wagner et al. [7] fabricated 3D printed auxetic metamaterials, according to two designs (reentrant and anti-tetrachiral honeycombs), using a multimaterial inkjet 3D printer on VeroWhitePlus RGD835; Yang et al. [8] realized geometrically-reconfigurable and mechanically-tunable lightweight metamaterials based on a SMP, using projection micro-stereolithography; Bodaghi et al. [9] developed multi-stable metamaterials with reversible thermomechanical shape memory by fused deposition modeling 3D printing. The studied structures allowed to obtain interesting shape shifting capabilities, such as the possibility to switching between negative and positive values of the Poisson's ratio, as found by Zhao et al. [10] on two- and three- dimensional periodic lattice metamaterials; the ability to switching between two patterns, as shown by Yuan et al. [11] on two-dimensional auxetic lattices made of an amorphous polymer and a flexible elastomer; or the tunable response of the two-and three-dimensional auxetics based on polylactide acid [12].

The idea of obtaining a sequential motion, with one or more intermediate configurations between the temporary and the permanent shape, is less studied for SMP auxetics, although this can be achieved by multi-material polymer 3D printer, or by using materials capable of a multiple SME. Multiple shape memory is a peculiar response shown in presence of more than one reversible transformation temperature (as in the case of blends or copolymers) or in presence of a single broad transition (either glass transition or melting temperature region). Only recently, Bodaghi et al. [15–16] used specific SMPs having three reversible transformation temperatures to engineer adaptive staples, springs, and two-dimensional self-folding lattices, by means of fused decomposition modeling 3D printing. To the authors' knowledge, no works focus on auxetics made of SMPs with a single broad transition. Material systems with a broad transition have proved to be particularly advantageous since their recovery process may be triggered at various temperatures, depending solely on the temperature at which the material is deformed, i.e. the so-called Temperature-Memory Effect (TME), and without requiring modification in the chemistry of the system. Thus, when deforming these materials in various steps at different deformation temperatures, the shape memory response is a multiple recovery process, in well-distinguished stages, each one triggered at a different temperature.

In the present work 4D printing and multiple SME are combined, by studying the possibility to exploit the TME, provided by a single commercial resin presenting a broad glass transition, towards the realization of auxetic metamaterials with programmable shape shifting ability. The realization of such a structure by means of StereoLithographic Apparatus (SLA) and the study of its mechanical response are first addressed, to later focus on its shape memory behavior, with special interest towards the influence of the deformation temperature as parameter to control the triggered response. Finally, experiments are presented aimed at illustrating, both quantitatively and qualitatively, the hierarchical, sequential shape change ability that may be exploited through the TME.

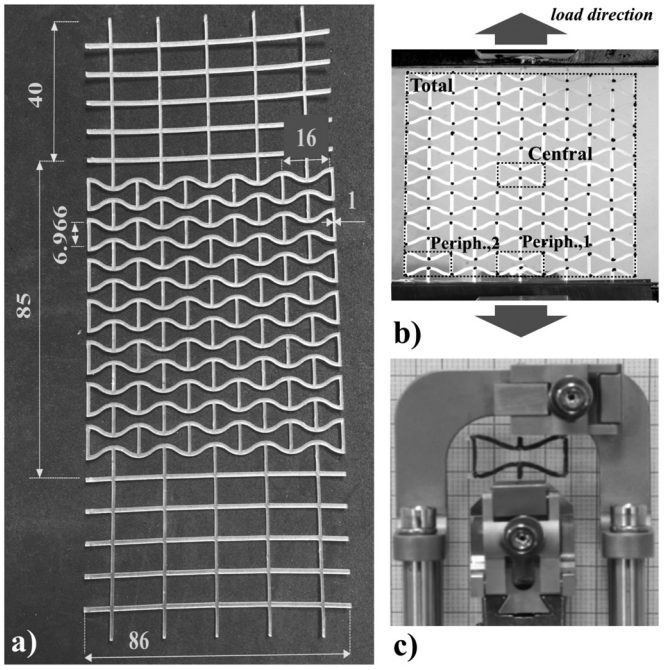

Fig. 1. (a) Investigated 3D printed structure, where thickness is equal to 0.8 mm and all dimensions are given in mm; (b) specimen configuration in the tensile tests, with load direction and position of the reference cells; (c) specimen configuration in the shape memory test.

2. Materials

2.1. Structure preparation

The investigated two-dimensional auxetic design is shown in Fig. 1a and was realized using SLA 3D printing.

More specifically, the Formlabs Form 2 printer (build volume of 145 × 145 × 175 mm and a 405 nm UV laser of 250 mW of power) was employed. The printer is able to cure photopolymer resins with a slice thickness resolution up to 25 μm and with laser spot of 140 μm. The structure was realized with a slice thickness of 50 μm and by using the photopolymer resin named Clear FLGPCL02, provided by Formlabs company.

The software PreForm (Formlabs) was used to orient and support the model. Model orientation was selected to avoid as much as possible support settlement on the repetitive cells, thus placing the long side of the model slightly angled with respect to the printing plate. In this way, at least the sides of each cell were self-sustained. Supports' contact points were set at 0.35 mm to avoid structure's impairment.

2.2. Thermal and mechanical characterization

Differential Scanning Calorimetry (DSC) analysis was first carried out by means of a DSC Q100 calorimeter (TA Instruments), in order to measure the glassy transition temperature, T_g, of the material. About 10 mg of material cut from the 3D printed specimen was subjected to the following thermal program: (i) a first heating run from −80 °C to 110 °C at 10 °C/min; (ii) a cooling run from 110 °C to −80 °C at 10 °C/min; (iii) a final heating run from −80 °C to 110 °C at 10 °C/min; nitrogen was used as purge gas.

Then, the structure was subjected to mechanical characterization by means of an electromechanic dynamometer (Instron Mod. 3366), in order to quantify the correlation between axial strain (i.e. parallel to the load direction) and transverse strain (i.e. perpendicular to the load direction) under uniaxial conditions. The

tests were carried out under tensile conditions at room temperature, according to the configuration displayed in Fig. 1b. A loading-unloading history was applied, up to a maximum displacement of 10 mm, with a crosshead speed equal to 20 mm/min.

The deformation was measured, via a marker tracking technique, for the whole structure as well as on single cells, in order to highlight possible differences between local and global behavior, due to confinement in the dynamometer grips. Several markers (black circles in Fig. 1b) were positioned on the entire structure knots and their displacement was tracked throughout the experiment by means of a camera with a sampling rate of 1 frame per second. A customized NI Labview software was used to carry out the marker tracking [17]. A calibration grid was used at the beginning of each test to compensate distortions due to camera lenses and perspective. The software preprocessed the images by applying proper binarization criterion, filters, and morphology operators in order to guarantee the best tracking results. Then, a blob analysis was performed to extract the calibrated blob centroids used for the marker displacements calculation. Finally, both X and Y displacements (with respect to the image axes) were saved for each tracked marker as a function of time. An ad-hoc Labview code allowed strain computation by applying a finite element theory and treating some of the markers as the nodes of an isoparametric finite element. Once the nodes of the elements of interest were defined, the software used the displacements of the nodes to automatically calculate the strain map on each element for each time instant. According to the 4-node isoparametric element theory, the element was intrinsically homogenous and needed to be associated to a homogenous unit on the grid corresponding to the elementary cell of the auxetic grid. For this reason, the 4-node isoparametric elements were always defined as multiple integers of the elementary cell. A total of 4 elements were used for these calculations (see Fig. 1b): the cell in the center of the structure (labeled as “Central”), a peripheral cell on the outer border and on the major symmetry axis (labeled as “Periph.,1″), a peripheral cell on the outer border and on the corner of the structure (labeled as “Periph.,2″) and the whole structure (labeled as “Total”).

2.3. Shape memory characterization

Four sets of shape memory tests were performed by means of a dynamic-mechanical analyzer (DMA Q800 - TA Instruments).

The first set of tests was carried out according to the thermo-mechanical cycle typically employed for SMPs, consisting of a “programming” step, followed by a recovery step. In particular, the effect of the “programming” temperature (or deformation temperature, T_{def}) on the shape memory response of the structure was evaluated. Accordingly, specimens consisting of a single cell were clamped at the extremities of the adjacent cell wall (Fig. 1c) and subjected to the following thermo-mechanical history: (i) heating from room temperature up to a given temperature, T_{def}; (ii) applying a tensile elongation equal to 3.5 mm (representing about 90% of the elongation required to have full cell opening); (iii) cooling to −15 °C (i.e. well below T_g) under fixed strain conditions (i.e. by maintaining the DMA arms position fixed); (iv) heating up to 110 °C at 1 °C/min under quasi stress-free conditions. During step iv, in fact, a constant load of moderate entity (0.001 N) was applied to the specimen, so to maintain proper contact and to monitor continuously the cell tensile displacement as a function of temperature. The test was repeated for different values of T_{def} equal to 20 °C, 40 °C, 60 °C, 80 °C, and 100 °C. Throughout the experiment, tensile displacement was quantified as the distance between the clamps under the hypothesis that such displacement mainly regards the cell and that the clamped cell walls contribution can be neglected.

The second set of tests was applied in order to explore the possibility of a sequential shape recovery ability as a consequence of a multi-step deformation history. The auxetic cell was subjected to a thermo-mechanical history similar to the previous one, but now based on a two-stage deformation: (i) heating from room temperature up to $T_{def\text{-}high}$ = 100 °C; (ii) applying a first tensile elongation equal to 1.75 mm (i.e. half of the elongation employed in the first set of tests); (iii) cooling to −20 °C under fixed strain conditions; (iv) heating up to $T_{def\text{-}low}$ = 40 °C and applying a second additional tensile elongation equal to 1.75 mm; (v) cooling to −20 °C under fixed strain conditions; (vi) heating up to 110 °C at 1 °C/min under quasi stress-free conditions.

The third set of tests were carried out in order to visually track the cell recovery along the heating ramp. Accordingly, the cell was subjected to a thermo-mechanical history similar to the first one, but now based on a progressive heating ramp: (i) heating from room temperature up to T_{def} = 100 °C; (ii) applying a tensile elongation equal to 3.5 mm; (iii) cooling to room temperature under fixed strain conditions; (iv) heating the specimen up to a given temperature at 1 °C/min under quasi stress-free conditions to promote partial recovery, and suddenly cooling to room temperature to fix the shape and taking a picture of the specimen configuration after this recovery; such a step is repeated heating at progressively higher temperatures until full recovery is achieved.

The fourth set of tests was aimed at evaluating the possibility of a sequential shape recovery for a more complex transformation, decoupling out-of-plane and in-plane deformation. A single cell was deformed by means of the following thermo-mechanical history, based on a two-stage deformation and a progressive heating ramp: (i) heating from room temperature up to $T_{def\text{-}high}$ = 100 °C; (ii) bending; (iii) cooling to −15 °C under this configuration; (iv) heating up to $T_{def\text{-}low}$ = 40 °C and applying a tensile elongation equal to 3.5 mm; (v) cooling to −15 °C under fixed strain conditions; (vi) heating up to a given temperature at 1 °C/min under quasi stress-free conditions to promote partial recovery, and suddenly cooling to room temperature to fix the shape and taking a picture of the specimen configuration after this recovery; such a step is repeated heating at progressively higher temperatures until full recovery is achieved.

In order to quantify the shape memory behavior, five quantities were introduced, as follows. The normalized displacement, Δ_{norm}, was defined as follows:

$$\Delta_{norm}(\%) = \Delta l/\Delta l_{app}\, x\, 100 \tag{1}$$

where: $\Delta l = l - l_0$; $\Delta l_{app} = l_{app} - l_0$; l is the distance between the clamps during the test; l_0 is the initial clamp distance; l_{app} is the clamp distance corresponding to the applied strain. Strain fixity (i.e. the percentage of elongation that is set in the deformed specimen after load removal), SF, was defined as follows:

$$SF(\%) = \Delta l_{unload}/\Delta l_{app}\ x\ 100 \tag{2}$$

where: $\Delta l_{unload} = l_{unload} - l_0$, l_{unload} is the clamp distance at load removal. Strain recovery (i.e. the percentage of applied elongation that may be recovered), SR, was defined according to the following relation:

$$SR(\%) = 100 - \left(\Delta l_{final}/\Delta l_{app}\, x\, 100\right) \tag{3}$$

where: $\Delta l_{final} = l_{final} - l_0$, l_{final} is the clamp distance at the end of the heating ramp. Recovery rate (i.e. the temperature derivative of the normalized displacement), RR, was evaluated as:

$$RR(\%/^{\circ}C) = d(\Delta l/\Delta l_{app})/dT\ x\ 100 \tag{4}$$

The normalized width, W_{norm}, was defined and employed only for the fourth set of tests, as follows:

$$W_{norm}(\%) = \Delta W/\Delta W_{app}\ x\ 100 \tag{5}$$

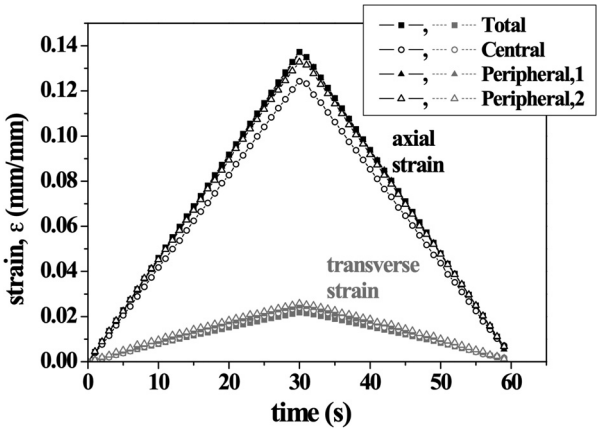

Fig. 2. Axial (i.e. parallel to the load direction) and transverse (i.e. perpendicular to the load direction) strain as a function of time along a loading-unloading test as measured on the whole auxetic structure (Total) and on single cells in various positions (Central; Peripheral,1, Peripheral,2).

where: $\Delta W = W - W_0$; $\Delta W_{app} = W_{app} - W_0$; W is the specimen overall width, measured frontally, during the test; W_0 is the initial overall width; W_{app} is the specimen overall width, measured frontally after bending.

3. Results and discussion

The results of DSC analysis revealed a widely distributed glass transition region, spreading over a temperature interval between 30 °C and 85 °C, with T_g at about 58 °C. This suggested that the key requirement for the TME was possibly met and motivated the mechanical and shape memory characterization described in Sections 2.2 and 2.3.

Fig. 2 shows the results of mechanical characterization in terms of axial and transverse strain as a function of time, along the performed loading-unloading ramp; strain values refer to the deformation of the isoparametric elements corresponding to the whole structure and to the various cells (Fig. 1b). All the curves show an expansion-contraction response during the loading-unloading cycle, with a similar trend for all the sampled areas, suggesting an overall homogeneous response on the local and global scale. A fairly linear correlation is evident between axial and transverse deformations. This allowed to easily measure Poisson's ratio, which displayed a negative value equal to about −0.18, thus demonstrating the auxetic behavior of the investigated structure.

Interestingly, the values of axial and transverse strain of the whole structure and of single cells were very similar, and this allowed to concentrate on the single cell to describe the shape memory response of the structure.

The results of the first set of shape memory tests are reported in Fig. 3a in terms of normalized displacement (Eq. (1)) versus temperature, for the cells deformed at T_{def} = 40 °C and T_{def} = 100 °C, as representative of the typical curves appearances for deformation below T_g and above T_g, respectively (curves with label T_{def} = 40 °C and T_{def} = 100 °C). The curves follow a sigmoidal trend, whose inflection point is defined by the inflection temperature, T_{flex}, that results equal to 47 °C and 85 °C for the cases T_{def} = 40 °C and T_{def} = 100 °C, respectively. Both specimens displayed almost full recovery, but with significant differences. While a high fixity level was found for T_{def} = 100 °C, a certain portion of strain was recovered during unloading for the specimen deformed at T_{def} = 40 °C (vertical arrow in Fig. 3a). More interestingly, the whole recovery process was affected by T_{def}, occurring, for the two cases, on different thermal regions and with a different distribution on the temperature scale; to better evidence this latter point, Fig. 3b displays the distribution of the recovery process on the temperature scale by means of the recovery rate (Eq. (4)). The whole recovery process was seen to move to higher temperatures as T_{def} increased; while the recovery for T_{def} = 40 °C (curve with label T_{def} = 40 °C) was associated with a broader recovery process, slowly onsetting right after cooling and occurring at its fastest rate in proximity of the deformation temperature, the specimen deformed at T_{def} = 100 °C (curve with label T_{def} = 100 °C) displayed a narrow recovery process onsetting at about 60 °C and gaining its fastest rate at 80 °C. Such a dependence on T_{def} is ascribed to the broad distribution of segmental relaxation motions, which are as well responsible of activating recovery. In particular, deformations at $T_{def} < T_g$ lead to a broad recovery process, which incorporates slower chain motions in the glassy region further than those ascribed to the main relaxation process; higher deformation temperatures lead to a recovery driven by entropic forces, that becomes effective when chains mobility increases on the basis of the main relaxation process.

Similar results were obtained at other deformation temperatures and are summarized in Table 1, in terms of strain fixity (Eq. (2)), strain recovery (Eq. (3)), and inflection temperature of the sigmoidal trend (T_{flex}).

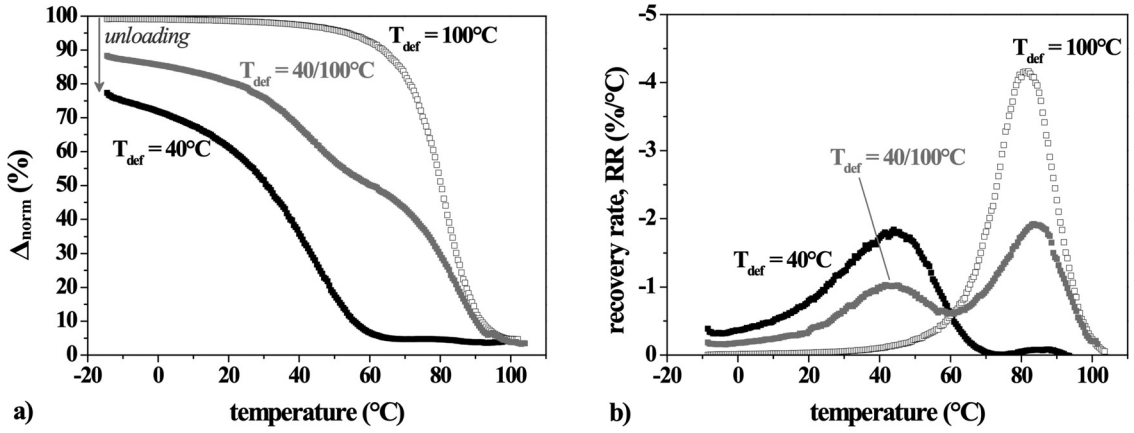

Fig. 3. (a) Normalized displacement, Δ_{norm}, and (b) recovery rate, RR, versus temperature curves for specimens deformed up to: full opening of the cell at 40 °C (label: T_{def} = 40 °C), full opening of the cell at 100 °C (label: T_{def} = 100 °C), and full opening with a two-step deformation history, half at 100 °C and half at 40 °C (label: T_{def} = 40/100 °C).

Table 1
Effects of the deformation temperature (T_{def}) on strain fixity, overall strain recovery and on the inflection point temperature of the sigmoidal recovery (T_{flex}), as measured on specimens subjected to a same amount of elongation (Δl_{app} = 3.5 mm).

T_{def} [°C]	Strain fixity, SF [%]	Strain recovery, SR [%]	T_{flex} [°C]
20	59	100	25
40	77	95	47
60	90	98	65
80	98	98	82
100	99	95	85

The strain fixity values show that only deformation temperatures close or above T_g allowed full fixation of the deformed configuration, while for T_{def} below T_g lower fixity values were found as temperature decreases: in particular, deformation at room temperature still allowed fixing more than half of the applied strain, and, interestingly, a slightly higher temperature (T_{def} = 40 °C) allowed fixing up to about 80% of the applied deformation. The results in Table 1 also show that, for all the deformation conditions, the applied strain was almost fully recovered (i.e. between 95% to 98%), the residual portion being presumably partly related to slipping in the DMA machine grips and to some flexural setting of the cell nodes in a more stable shape. Finally, the inflection point temperature, T_{flex}, was seen to increase with deformation temperature to finally appearing to approach a steady value around 85 °C for deformation above 80 °C. Interestingly, for deformations up to 80 °C, T_{flex} appeared to be strongly related to the deformation temperature and assumed a value approximately equal to T_{def} + 5 °C.

All the achieved results suggest that T_{def} can be used as a functional parameter to govern the transformation temperature, as in the typical phenomenology of the so-called TME. A further potential exploitation of such an effect relies on the possibility to obtain multiple and sequential transformations, as a consequence of a specific thermo-mechanical history, as recently explored for bulk systems based on the same photopolymer [18].

The possibility to use T_{def} as a functional parameter is clearly evidenced by the results of the second set of shape memory tests. In these tests, the deformation temperatures for the two-step deformation were chosen as 40 °C and 100 °C, since the distribution of the recovery processes, shown in Fig. 3b, revealed a good degree of separation of the corresponding recovery processes on the temperature scale. The recovery trace of the specimen after this double stretching is reported in Fig. 3a and b, in terms of normalized displacement (Eq. (1)) and recovery rate (Eq. (4)), respectively (curves with label T_{def} = 40/100 °C), so to be properly compared with the curves of specimens completely deformed at a single temperature. From Fig. 3a and b, it is possible to see that the recovery process of the two-step deformed cell occurred as two sequential sub-processes, as demonstrated by the double inflection of the recovery curve and by the double peak of the recovery rate curve. Interestingly, these two processes were seen to be strongly related to the single step recovery curves. In fact, the recovery rate distribution of the two sub-processes and the peak position in Fig. 3b is the same of those of the specimen deformed at T_{def} = 40 °C and T_{def} = 100 °C. Further, the two processes seemed to both cover 50% of the entire recovery process: the high-temperature process seemed to be related to a sigmoidal recovery that onset at around 50% and lead to full recovery, consistently to the high fixity and recovery ability of the specimen deformed at T_{def} = 100 °C; the low-temperature process, as for the specimen deformed at T_{def} = 40 °C, seemed to be represented by a recovery process with a reduced fixity, and it is interesting to observe that the portion of strain recovered at unloading was actually about

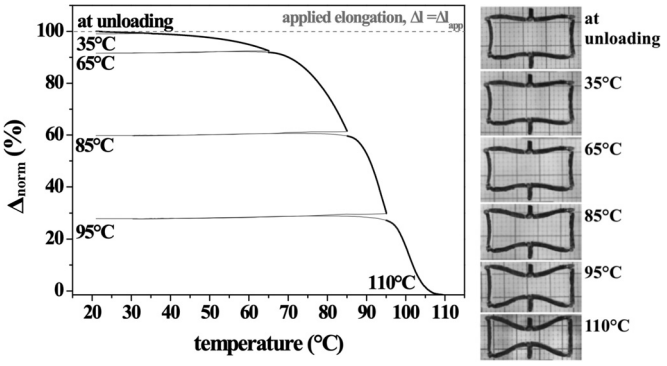

Fig. 4. Shape memory response of the cell after a deformation at T_{def} = 100 °C in the recovery step of the third set of experiments, with sampling of the specimen shape at various temperatures in order to have visual representation of the effect.

half of that recovered by the curve of the specimen deformed at 40 °C.

The results of the third set of shape memory tests are reported in Fig. 4 and allow to visualize the progressive reduction of strain with temperature as well as the deformed configuration for each sampling step. Fig. 4 suggests, both visually and quantitatively, the possibility to fix a fully-deployed shape at unloading at T_{def} = 100 °C. The normalized displacement value at unloading indicates that strain fixity (Eq. (2)) was 100% under these deformation conditions and that this shape was maintained practically unchanged up to 65 °C. The recovery occurred through a contraction of the cell, and the process could be described as a sigmoidal function of temperature, with a steepest recovery slope at 95 °C, in correspondence of the curve inflection point. At the end of the heating ramp, the cell recovered its undeformed shape (Δ_{norm} = 0%; SR = 100%), with an overall area contraction of about 42%.

In order to provide evidence of the TME on a more complex case, the fourth set of shape memory experiments were conducted to decouple the shape evolution in out-of-plane flexural motions and in-plane contraction of the cell on the temperature scale. Again, the deformation temperatures for the two-step deformation were chosen as 40 °C and 100 °C. The recovery process is visually described in the pictures of Fig. 5a and b, and in the recovery curves of Fig. 5c Eqs. (1) and (5), which represents how the in-plane elongation (Δ_{norm}) and the out-of-plane flexure (W_{norm}) recover as a function of the increasing temperature. The recovery of the two deformations was seen to occur on significantly different regions: the in-plane recovery of the cell takes place earlier, onsetting right after unloading and being completed at about 60 °C; the out-of-plane recovery of the cell starts at about 45 °C, when the in-plane process is almost complete (about 80%), and gets accomplished at 100 °C. This finding suggests that the two processes are fully dictated by the programming history and supports the validity of the TME to achieve thermally-triggered sequential shape variations.

Finally, it is important to point out that the role of printing parameters on the shape memory response was not investigated. Given a specific photopolymer material formulation, the microstructure of the 3D printed material is highly affected by SLA printing parameters as laser power, scan velocity, radius of the beam, exposure time, and cure depth. Most of the SLA printer available on the market don't allow a direct modification of such parameters, being calibrated to obtain the best surface quality of the 3D printed object. Only indirect parameters can be tuned, like layer height or speed/quality balance. In our case, those parameters – along with model's orientation and support strategy - were tuned only to achieve the highest geometrical accuracy of the final

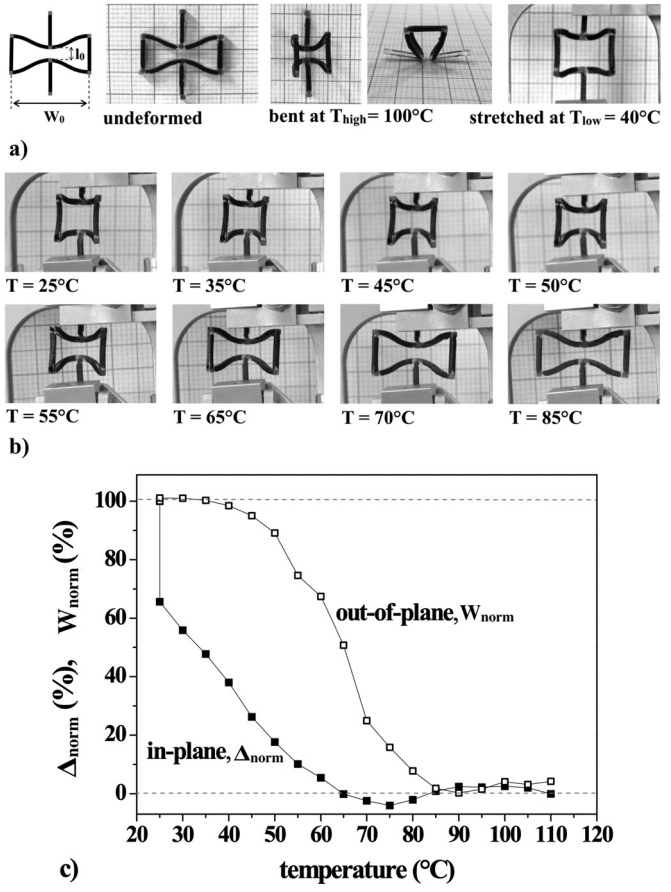

Fig. 5. (a) Two-step deformation, (b) shape recovery, and (c) recovery curves for a single cell subjected to a two-step programming consisting of an early out-of-plane bending at $T_{def\text{-}high}$ = 100 °C and a subsequent stretching at $T_{def\text{-}low}$ = 40 °C.

model. As a future step, it would be interesting to investigate the role of printing parameters on the shape memory response and the possibility to tune it accordingly.

4. Conclusions

The present paper has investigated 4D printing of a SMP-based auxetic structure. Its mechanical behavior, measured in loading-unloading ramp, showed the typical auxetic response, and, thanks to the linear correlation between axial and transverse strain, a negative Poisson's ratio equal to about −0.18 was quantified. Shape memory tests carried out on single cells by means of a properly-defined protocol, allowed to verify an interesting shape memory behavior, featuring, for high elongation of the cell, high values of fixity and practically complete recovery of the original shape. Further, as a consequence of a broad glass transition region, the material presented the so-called TME, i.e. the region of thermal recovery moved to higher temperatures as the deformation temperature increased, allowing to employ deformation temperature to tune the thermal region that triggered the shape memory response. Thanks to the TME, auxetics were programmed to achieve thermally-triggered hierarchical motions and self-deployment capabilities. In particular, even complex responses, such as sequential in-plane and out-of-plane motions, were shown to be easily controlled simply through a proper definition of the thermo-mechanical history. The possibility of coupling different types of motions/responses (e.g. synclastic curvature, in-plane elongations) may be beneficial for various applications, as soft robotics or biomedical components. It is worth highlighting that the investigated design, resembling re-entrant honeycomb auxetic cellular structures, was chosen thanks to its simple manufacturability and not to achieve Poisson's ratios lower than those currently available from the literature. However, the obtained results are very general and can be applied to any two-dimensional or three-dimensional auxetic geometry.

Declaration of Competing Interest

The authors declare that they have no known competing financial interests or personal relationships that could have appeared to influence the work reported in this paper.

Acknowledgements

This work was partially supported by Regione Lombardia through the project "MADE4LO - Metal ADditivE for LOmbardy" (No. 240963) within the POR FESR 2014–2020 program and by the *Italian Minister of University and Research through the project "A BRIDGE TO THE FUTURE: Computational methods, innovative applications, experimental validations of new materials and technologies" (No. 2017L7X3CS) within the PRIN 2017 program. The authors kindly acknowledge Mrs. Marica Bianchi for contributing to shape memory characterization.*

References

[1] H. Kolken, A. Zadpoor, Auxetic mechanical metamaterials, RSC Adv. 7 (2017) 5111–5129.
[2] M. Mirzaali, S. Janbaz, M. Strano, L. Vergani, A. Zadpoor, Shape-matching soft mechanical metamaterials, Sci Rep 8 (2018) 1–7.
[3] J. Rossiter, K. Takashima, F. Scarpa, P. Walters, T. Mukai, Shape memory polymer hexachiral auxetic structures with tunable stiffness, Smart Mater. Struct. 23 (2014) 045007–1-11.
[4] M. Berwind, A. Kamas, C. Eberl, A hierarchical programmable mechanical metamaterial unit cell showing metastable shape memory, Adv. Eng. Mater. 1800771 (2018) 1–6.
[5] S. Jacobs, C. Coconnier, D. DiMaio, F. Scarpa, M. Toso, J. Martinez, Deployable auxetic shape memory alloy cellular antenna demonstrator: design, manufacturing and modal testing, Smart Mater. Struct. 21 (2012) 075013–1-12.
[6] X. Kuang, D. Roach, J. Wu, C. Hamel, Z. Ding, T. Wang, M. Dunn, H. Qi, Advances in 4D printing: materials and applications, Adv. Funct. Mater. 29 (2019) 1805290–1-23.
[7] M. Wagner, T. Chen, K. Shea, Large shape transforming 4D auxetic structures, 3D Print, Add. Manuf. 4 (2017) 133–141.
[8] C. Yang, M. Boorugu, A. Dopp, J. Ren, R. Martin, D. Han, W. Choi, H. Lee, 4D Printing reconfigurable, deployable and mechanically tunable metamaterials, Mater. Horiz. (2019) 1–8.
[9] M. Bodaghi, W. Liao, 4D printed tunable mechanical metamaterials with shape memory operations, Smart Mater. Struct. 28 (2019) 045019–1-15.
[10] Z. Zhao, C. Yuan, M. Lei, L. Yang, Q. Zhang, H. Chen, H. Qi, D. Fang, Three-Dimensionally printed mechanical metamaterials with thermally tunable auxetic behavior, Phys. Rev. Appl. 11 (2019) 044074.
[11] C. Yuan, X. Mu, C. Dunn, J. Haidar, T. Wang, H. Qi, Thermomechanically triggered two-stage pattern switching of 2D lattices for adaptive structures, Adv. Funct. Mater. 28 (2018) 1705727–1-9.
[12] M. Lei, W. Hong, Z. Zhao, C. Hamel, M. Chen, H. Lu, H. Qi, 3D printing of auxetic metamaterials with digitally reprogrammable shape, ACS Appl. Mater. Interfaces 11 (2019) 22768–22776.
[13] J. Jackson, M. Messner, N. Dudukovic, W. Smith, L. Bekker, B. Moran, A. Golobic, A. Pascall, E. Duoss, K. Loh, C. Spadaccini, Field responsive mechanical metamaterials, Sci Adv. 4 (2018) eaau6419-1-9.
[14] S. Li, H. Hassanin, M. Attallah, N. Adkins, K. Ess, The development of TiNi-based negative Poisson's ratio structure using selective laser melting, Acta Mater. 105 (2016) 75–83.
[15] M. Bodaghi, A. Damanpack, W. Liao, Adaptive metamaterials by functionally graded 4D printing, Mater. Des. 135 (2017) 26–36.
[16] M. Bodaghi, A. Damanpack, W. Liao, Triple shape memory polymers by 4D printing, Smart Mater. Struct. 27 (2016) 065010–1-18.
[17] A. Avanzini, D. Battini, Integrated experimental and numerical comparison of different approaches for planar biaxial testing of a hyperelastic material, Adv. Mater. Sci. Eng. (2016) 6014129-1-12.
[18] N. Inverardi, S. Pandini, F. Bignotti, G. Scalet, S. Marconi, F. Auricchio, Temperature-memory effect in 3D printed photopolymers with broad glass transition (Conference paper), AIP Conf. Proc. 1981 (2018) 020146.